Experimental control of high-dimensional chaos: The driven double pendulum

David J. Christini,[1] James J. Collins,[1] and Paul S. Linsay[2]
[1]*NeuroMuscular Research Center and Department of Biomedical Engineering, Boston University, 44 Cummington Street, Boston, Massachusetts 02215*
[2]*Plasma Fusion Center, Massachusetts Institute of Technology, 175 Albany Street, Cambridge, Massachusetts 02139*
(Received 10 June 1996)

Chaos control techniques exploit the sensitivity of chaos to initial conditions by applying feedback perturbations to an accessible system parameter. Most methods apply only one perturbation per period and are thus susceptible to control failure when applied to highly unstable systems. Here we extend a recently developed model-independent, quasicontinuous chaos control technique to stabilize a high-dimensional chaotic system: the driven double pendulum. [S1063-651X(96)12011-0]

PACS number(s): 05.45.+b, 07.05.Dz

The widespread existence of chaotic dynamics in physical systems has fostered great interest in the development of practical chaos control techniques. The original feedback chaos control technique developed by Ott, Grebogi, and Yorke [1] is based on the fact that there is an infinite number of unstable periodic orbits (UPO's) embedded within a chaotic attractor. The Ott-Grebogi-Yorke (OGY) approach exploits the sensitivity of chaos to initial conditions by making small time-dependent perturbations to an accessible system wide parameter such that the system's state point is attracted towards the stable direction of a targeted UPO. The OGY technique is practical from an experimental standpoint because it requires no analytical model of the system: all necessary dynamics are estimated from time series measurements made on the system.

The OGY approach and similar model-independent feedback control techniques have been successfully used to control a wide range of experimental systems [2]. However, because the OGY technique is limited to the control of low-dimensional systems, it is not applicable to the majority of real-world (i.e., high-dimensional) systems. Several high-dimensional control algorithms [3], including one recently used to control a magnetoelastic ribbon in a state of high-dimensional chaos [4,5], have been developed to overcome this limitation. However, because these techniques, like the OGY approach, apply control perturbations only once per period, amplification of noise and measurement errors by highly unstable systems may lead to control failure [6]. Recently, a quasicontinuous chaos control technique known as the *local control method* [6,7] has been developed to reduce the likelihood of control failure by applying several control perturbations per period. This model-independent technique has been successfully used to control two low-dimensional chaotic systems: a driven single pendulum [7,8] and a driven bronze ribbon [7]. In this study, we extend the local control method to stabilize a high-dimensional chaotic system: the driven double pendulum.

During each drive period, the local control method attempts to stabilize a targeted UPO by applying N control perturbations δp to an accessible parameter p, such that $p=\overline{p}+\delta p$, where $\overline{p}$ is the initial value of p. To determine the perturbations required to stabilize the targeted UPO, this method introduces N successive Poincaré sections $\Sigma^n, n=0,\ldots,(N-1)$, where Σ^n is intersected by $\mathbf{z}^n$, the nth system state vector. The local control method developed in Refs. [6,7] utilizes a state vector that is entirely comprised of measured variables. Here we extend the method by using time delay coordinates [9], where $\mathbf{z}^n$ is comprised of both current and former values of measured variables. With time delay coordinates, $\mathbf{z}^{n+1}$ is a function of $\mathbf{z}^n$ and all values of p during the delay lag m (i.e., $p^n, p^{n-1}, \ldots, p^{n-m+1}$) [10]. Thus the mapping $\mathbf{P}^{(n,n+1)}$ from Σ^n to Σ^{n+1} is

$$\mathbf{z}^{n+1}=\mathbf{P}^{(n,n+1)}(\mathbf{z}^n,p^n,p^{n-1},\ldots,p^{n-m+1}). \tag{1}$$

Setting $\delta\mathbf{z}^n=\mathbf{z}^n-\mathbf{z}_F^n$ where $\mathbf{z}_F^n\in\Sigma^n$ is the intersection of the UPO with Σ^n, the linear approximation of $\mathbf{P}^{(n,n+1)}$ around $\mathbf{z}_F^n$ and $\overline{p}$ gives

$$\delta\mathbf{z}^{n+1}=\mathbf{A}^n\,\delta\mathbf{z}^n+\sum_{j=0}^{m-1}\mathbf{w}_j^n\,\delta p^{n-j}, \tag{2}$$

where

$$\mathbf{A}^n=D_{\mathbf{z}^n}\mathbf{P}^{(n,n+1)}(\mathbf{z}_F^n,\overline{p)}, \tag{3}$$

$$\mathbf{w}_j^n=\frac{\delta\mathbf{P}^{(n,n+1)}(\mathbf{z}_F^n,\overline{p)}}{\delta p^{n-j}}. \tag{4}$$

The Jacobian matrix $\mathbf{A}^n$ represents the linearization of $\mathbf{P}^{(n,n+1)}$ around $\mathbf{z}_F^n$ while $\mathbf{w}_j^n$ are vectors that measure the sensitivity of $\mathbf{P}^{(n,n+1)}$ to current $(j=0)$ and former $(j>0)$ parameter perturbations.

Computation of the local control parameter perturbation δp utilizes the fact that $\mathbf{A}^n$ deforms a hypersphere surrounding $\mathbf{z}_F^n$ in Σ^n into a hyperellipsoid surrounding $\mathbf{z}_F^{n+1}$ in Σ^{n+1}. Singular value decomposition of $\mathbf{A}^n$ ($\mathbf{A}^n=\mathbf{U}^n\mathbf{W}^n\mathbf{V}^{nT}$, where the superscript T denotes transpose) is used to obtain the Σ^n hypersphere vector $\mathbf{v}_u^n$ (the direction of maximal stretching), which is mapped onto the largest axis of the Σ^{n+1} hyperellipsoid. Thus the vector $\mathbf{v}_u^n$ is the column vector of $\mathbf{V}^n$ corresponding to the largest singular value μ_u^n of $\mathbf{W}^n$. Once $\mathbf{z}^n$ enters into the hypersphere neighborhood surrounding $\mathbf{z}_F^n$ the local control method attempts to constrain the system within the target UPO by selecting

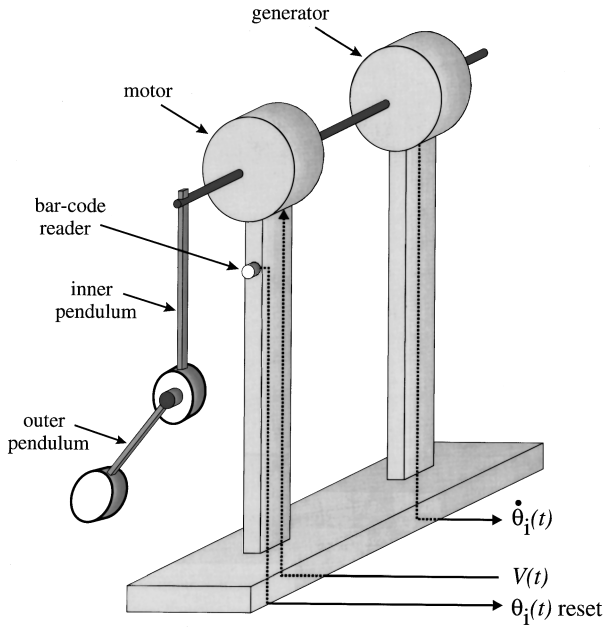

FIG. 1. Schematic of the driven double pendulum setup. The inner and outer pendulums are aluminum bars weighted on one end (the distal end). Each pendulum has full rotational freedom about an axis passing through its proximal end. The outer pendulum's rotational axis passes through the center of the inner pendulum weight and is in the same direction as an electric motor axle that serves as the inner pendulum rotational axis. The electric motor generates an external torque that is dependent on a sinusoidal drive voltage $V(t)=A\sin(2\pi ft)+p$. The angular velocity $\dot{\theta}_i$ of the inner pendulum is measured by a generator whose axle is linked to the axle of the motor. The $\dot{\theta}_i$ signal is integrated by an electronic circuit (not shown) to provide the inner pendulum angle θ_i.

δp^n such that the projection of $\delta\mathbf{z}$ onto $\mathbf{v}_u$ decreases by a factor of $(1-\rho)$ during each control step, i.e.,

$$\mathbf{v}_u^{n+1T}\delta\mathbf{z}^{n+1}=(1-\rho)\mathbf{v}_u^{nT}\delta\mathbf{z}^n. \tag{5}$$

Thus the local control formula is obtained by inserting Eq. (5) into Eq. (2):

$$\delta p^n=\frac{(1-\rho)\mathbf{v}_u^{nT}\delta\mathbf{z}^n-\mathbf{v}_u^{n+1T}\left(\mathbf{A}^n\delta\mathbf{z}^n+\sum_{j=0}^{m-1}\mathbf{w}_j^n\delta p^{n-j}\right)}{\mathbf{v}_u^{n+1T}\mathbf{w}_0^n}. \tag{6}$$

As in Ref. [7], we limit the applied perturbation to $|\delta p^n|\leqslant\delta p_{\max}$ [11], i.e.,

$$\delta p^n=\begin{cases}\delta p^n & \text{for } |\delta p^n|\leqslant\delta p_{\max}\\ \operatorname{sgn}(\delta p^n)\,\delta p_{\max} & \text{for } |\delta p^n|>\delta p_{\max}.\end{cases} \tag{7}$$

The setup for the driven double pendulum control experiment is shown in Fig. 1. The electric drive motor is powered by a sinusoidal voltage $V(t)=A\sin(2\pi ft)+p$. For this experiment, $A=1.3$ V, $f=1.2$ Hz, and p is a dc torque that is used as the accessible control parameter ($\overline{p}=0.0$ V). The angular velocity $\dot{\theta}_i$ of the inner pendulum is measured by an electronic circuit connected to the voltage output of a generator, whose axle is linked to the axle of the drive motor. The electronic circuit then integrates $\dot{\theta}_i$ to provide the inner pendulum angle θ_i. Whenever the pendulum swings through $\theta_i=0$, a vertical line on the back of the inner pendulum arm is detected by a bar-code reader. The bar-code reader triggers an integration reset ($\theta_i=0$) to constrain $-2\pi<\theta_i<2\pi$. The $\dot{\theta}_i$, θ_i, and V signals are scanned via analog-to-digital conversion into a PowerMacintosh 7100/80 computer at a sampling rate of Nf ($N=20$), the same rate at which control perturbations δp are returned via digital-to-analog conversion from the computer to the drive motor.

To locate the target UPO on which control was to be attempted, $\dot{\theta}_i$ and θ_i were recorded from the driven double pendulum for 7500 drive cycles with $\delta p=0.0$ V. The driven double pendulum has five degrees of freedom (the drive phase $\dot{\theta}_i$, θ_i, $\dot{\theta}_o$, and θ_o, where $\dot{\theta}_o$ and θ_o represent the angular velocity and angle of the outer pendulum, respectively). In this experiment, $\dot{\theta}_o$ and θ_o were not available via measurement. Thus we used a time-delay coordinate embedding, comprised of two $\{\dot{\theta}_i,\ \theta_i\}$ pairs, to reconstruct the pendulum dynamics: $\mathbf{z}^n=(\dot{\theta}_i^{\,n},\theta_i^n,\dot{\theta}_i^{\,n-m},\theta_i^{n-m})^T$, where $m=5$. (This value was selected because the first minimum in the mutual information [12] for $\dot{\theta}_i$ occurred at five samples.) The method of false nearest neighbors [13] indicated that using three $\{\dot{\theta}_i,\ \theta_i\}$ pairs for the time-delay embedding produced the optimal attractor reconstruction (false nearest-neighbor percentage of 8.0%). However, this was only a 2.7% improvement over using two $\{\dot{\theta}_i,\ \theta_i\}$ pairs for the time-delay embedding (false nearest-neighbor percentage of 10.7%). Consequently, we used two $\{\dot{\theta}_i,\ \theta_i\}$ pairs for the time-delay embedding in order to reduce the complexity of the control intervention computations [Eq. (6)]. The entire data record was searched for period-1 orbits, i.e., segments of the time series that satisfied $|(\dot{\theta}_i^n-\dot{\theta}_i^{n+N})/\dot{\theta}_i^{\,n}|<0.025$ and $|(\theta_i^n-\theta_i^{n+N})/\theta_i^n|<0.025$. Because more than one unique UPO can exist for a given period, each period-1 orbit was classified as either (i) a unique orbit or (ii) a recurrence of a previously identified orbit. An orbit was considered recurrent if it had the same drive phase as a previously identified orbit and if each of its $\dot{\theta}_i^n$ and θ_i^n were within 5% of those of the previously identified orbit. Each orbit with at least ten recurrences was considered to be a valid UPO. The components $\mathbf{z}_F^n$ of each valid UPO were computed as the averages of all recurrences of $\dot{\theta}_i^n$, θ_i^n $\dot{\theta}_i^{n-m}$ and θ_i^{n-m}. Figure 2 shows the double pendulum's libration UPO, which was selected for control in this study because it had more recurrences (215 recurrences) than any other UPO.

The Jacobian matrices and sensitivity vectors of Eq. (6) were estimated from a second recording during which a single δp perturbation was applied each period [14]. The duration of each perturbation was $1/(Nf)$ (i.e., 0.04 s, which was the same duration used during control) and each amplitude was randomly selected as -0.3, -0.15, 0.0, $+0.15$, or $+0.3$ V. During the recording, the application of the perturbations was timed such that each $n\in N$ received 3500 perturbations. After the recording, the Jacobian matrices and sensitivity vectors were estimated from the nearest neighbors of each $\mathbf{z}_F^n$. Because the sensitivity vectors are only affected

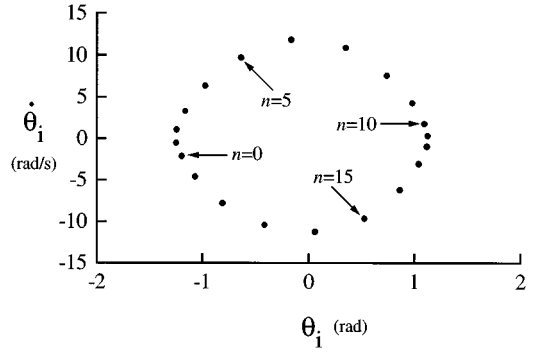

FIG. 2. Libration unstable periodic orbit (UPO), shown in the θ_i-$\dot{\theta}_i$ plane, for the driven double pendulum of Fig. 1.

by perturbations that occur during the delay lag m, the nearest-neighbor search was limited to those vectors that followed an applied perturbation by fewer than m lags. For each $n \in N$, the 40 nearest neighbors of $\mathbf{z}_F^n$, their corresponding $\mathbf{z}_F^{n+1}$ and the corresponding perturbations δp^{n-j} (where j equals the number of scans between the perturbation and the nearest neighbor) were simultaneously fit to Eq. (2) to estimate $\mathbf{A}^n$ and $\mathbf{w}_j^n$ $(j=0,1,\ldots,m-1)$.

The Lyapunov numbers ($\lambda_1=138.0, \lambda_2=-2.8, \lambda_3=0.3$, and $\lambda_4=1.0\times10^{-4}$) [15] for the target UPO shown in Fig. 2 indicate that the orbit has two unstable directions [16]. Figure 3 shows the singular values μ^n for each $\mathbf{A}^n$ of the target UPO. The variation of the singular values around the orbit indicates that orbit stability is dependent on n. For each $n \in N$, there are at least two unstable directions ($\mu>1.0$). It should also be noted that each of the $\mathbf{A}^n$ Jacobian matrices estimated from Eq. (2) was characterized by at least two complex eigenvalues. Thus a local control approach that employs eigenvalues, rather than singular value decomposition, would be inappropriate for this system and other systems with complex eigenvalues for $\mathbf{A}^n$.

Figure 4 shows local control of the inner pendulum angular velocity, along with the corresponding parameter perturbations, for the target UPO shown in Fig. 2. Control initiation occurred when $\mathbf{z}^n$ entered into the hypersphere

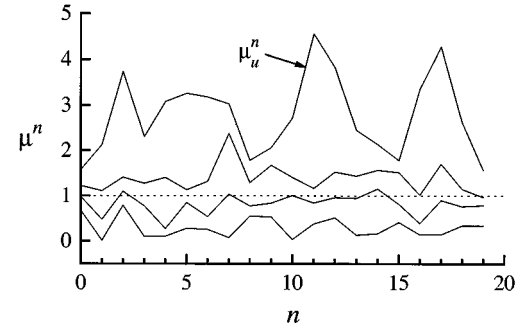

FIG. 3. Singular values μ^n of $\mathbf{A}^n$ for the UPO shown in Fig. 2. Values of $\mu>1.0$ indicate an unstable (expanding) direction, while values of $\mu<1.0$ indicate a stable (contracting) direction. The largest singular value μ_u^n corresponds to the direction of maximum stretching.

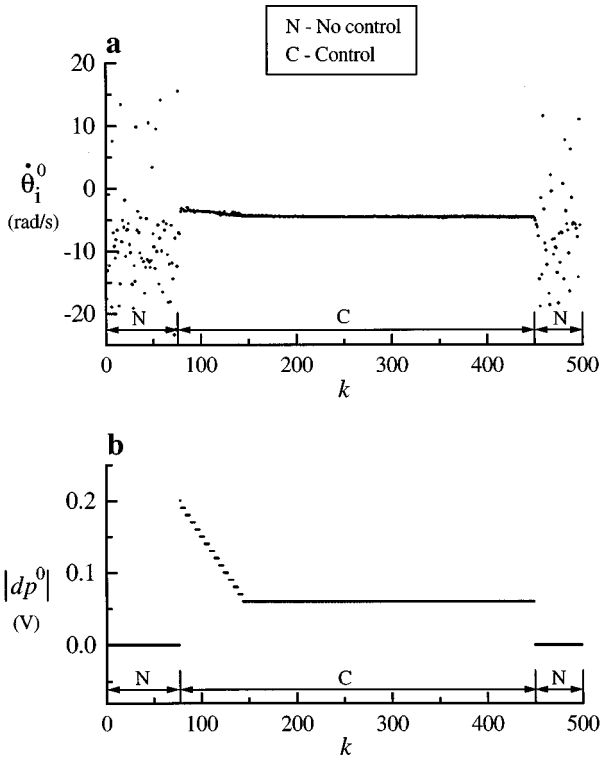

FIG. 4. Local control of the UPO shown in Fig. 2. (a) $\dot{\theta}_i^0$ (i.e., $\dot{\theta}_i$ for the first Poincaré section Σ^0) versus cycle number k. (b) Absolute value of the corresponding control perturbations δp^0 computed by Eqs. (6) and (7) with $\rho=0.15$. The duration of each perturbation was 0.04 s. Control was inactive ($\delta p=0.0$) until $\mathbf{z}^n$ entered into the hypersphere neighborhood surrounding $\mathbf{z}_F^n$ at $k=77$. Control was then activated with $\delta p_{\max}=0.2$ V. Subsequently, $\delta p_{\max}$ was uniformly decreased to $\delta p_{\max}=0.06$ V. At $k=450$, control was turned off and the double pendulum resumed its chaotic motion. The respective control stages are annotated in (a) and (b).

surrounding $\mathbf{z}_F^n$. The initial size of the hypersphere (corresponding to a maximum allowable parameter perturbation of $\delta p_{\max}=0.2$ V) was selected to allow a timely entry into the $\mathbf{z}_F^n$ neighborhood. Once control was obtained, $\delta p_{\max}$ was uniformly decreased to a value of approximately 5% of the drive amplitude A. Control could be maintained indefinitely, even with these small perturbations. The stabilized orbit never exactly matched the target UPO. (This was consistent with Ref. [7].) Thus the control perturbations computed by Eq. (6) consistently exceeded $\delta p_{\max}$ and were capped by Eq. (7). Once control was turned off, the double pendulum quickly resumed its chaotic motion (Fig. 4).

In order to demonstrate the robustness of control, ''measurement'' noise was added to each component of $\mathbf{z}^n$, i.e., $\mathbf{z}^n=(\dot{\theta}_i^n+\epsilon\xi_1^n, \theta_i^n+\epsilon\xi_2^n, \dot{\theta}_i^{n-m}+\epsilon\xi_3^n, \theta_i^{n-m}+\epsilon\xi_4^n)^T$, where $\xi_1^n, \xi_2^n, \xi_3^n$, and ξ_4^n are independent random variables uniformly distributed in $[-1,1]$ and ϵ is a constant. At $\delta p_{\max}=0.06$ V, control could be maintained indefinitely for $\epsilon=0.05A$. Interestingly, control could also be maintained (in the absence of additive noise) even if former perturbations were excluded from Eq. (6), i.e., $w_j^n=0$ for $j>0$, thus further indicating the robustness of the local control method.

In this study, we have demonstrated that a delay coordinate extension of the local control method can be used to control an experimental high-dimensional chaotic system. These developments may further open up real-world applications of chaos control. For example, the approach used in the present study may be particularly appropriate for mechanical and biological [17] systems, which are often high dimensional.

This work was supported by the National Science Foundation (J.J.C. and D.J.C.) and the Office of Naval Research (P.S.L.).

[1] E. Ott, C. Grebogi, and J. A. Yorke, Phys. Rev. Lett. **64**, 1196 (1990).

[2] W. L. Ditto, S. N. Rauseo, and M. L. Spano, Phys. Rev. Lett. **65**, 3211 (1990); E. R. Hunt, *ibid.* **67**, 1953 (1991); B. Peng, V. Petrov, and K. Showalter, J. Phys. Chem. **95**, 4957 (1991); R. Roy, T. W. Murphy, T. D. Maier, Z. Gills, and E. R. Hunt, Phys. Rev. Lett. **68**, 1259 (1992); V. Petrov, V. Gáspár, J. Masere, and K. Showalter, Nature **361**, 240 (1993).

[3] D. Auerbach, C. Grebogi, E. Ott, and J. A. Yorke, Phys. Rev. Lett. **69**, 3479 (1992); F. J. Romeiras, C. Grebogi, E. Ott, and W. P. Dayawansa, Physica D **58**, 165 (1992); P. So and E. Ott, Phys. Rev. E **51**, 2955 (1995).

[4] V. In, W. L. Ditto, M. Ding, W. Yang, M. L. Spano, and B. J. Gluckman (unpublished).

[5] M. Ding, W. Yang, V. In, W. L. Ditto, M. L. Spano, and B. J. Gluckman, Phys. Rev. E **53**, 4334 (1996).

[6] B. Hübinger, R. Doerner, and W. Martienssen, Z. Phys. B **90**, 103 (1993).

[7] B. Hübinger, R. Doerner, W. Martienssen, M. Herdering, R. Pitka, and U. Dressler, Phys. Rev. E **50**, 932 (1994).

[8] R. Jan de Korte, J. C. Schouten, and C. M. van den Bleek, Phys. Rev. E **52**, 3358 (1995).

[9] In a different manner, Ref. [8] also extends the local control method by using time delay coordinates.

[10] U. Dressler and G. Nitsche, Phys. Rev. Lett. **68**, 1 (1992).

[11] $\delta p_{\max}$ dictates how close $\mathbf{z}^n$ must come to $\mathbf{z}_F^n$ (i.e., the size of the hypersphere neighborhood) before control can be initiated.

[12] A. M. Fraser and H. L. Swinney, Phys. Rev. A **33**, 1134 (1986).

[13] M. B. Kennel, R. Brown, and H. D. I. Abarbanel, Phys. Rev. A **45**, 3403 (1992).

[14] In previous local control [7,8] applications, a different approach was employed: one recording (with no perturbations) was used for Jacobian estimation and a separate recording (with perturbations) was used to estimate the sensitivity vectors.

[15] The Lyapunov numbers were computed by a method utilizing *QR* decomposition, as described by J. P. Eckmann and D. Ruelle, Rev. Mod. Phys. **57**, 617 (1985).

[16] Although the control law of Eq. (6) considers only the largest unstable direction, the magnitude of the second unstable direction (characterized by λ_2) was not large enough to cause control failure.

[17] A. Garfinkel, M. L. Spano, W. L. Ditto, and J. N. Weiss, Science **257**, 1230 (1992); S. J. Schiff, K. Jerger, D. H. Duong, T. Chang, M. L. Spano, and W. L. Ditto, Nature **370**, 615 (1994); D. J. Christini and J. J. Collins, Phys. Rev. Lett. **75**, 2782 (1995); Phys. Rev. E **53**, 49 (1996).